

Exploring neutrino parameters with a beta-beam experiment from FNAL to DUSEL

Sanjib Kumar Agarwalla^{1,*} and Patrick Huber^{1,†}

¹*Department of Physics, Virginia Tech, Blacksburg, VA 24061, USA*

Abstract

We discuss in detail the physics reach of an experimental set-up where electron neutrinos (anti-neutrinos) produced in a beta-beam facility at Fermi National Accelerator Laboratory (FNAL) are sent, over a distance of $L \simeq 1300$ km, to the Deep Underground Science and Engineering Laboratory (DUSEL). A 300 kt Water Cherenkov (WC) detector and a 50 kt Liquid Argon Time Projection Chamber (LArTPC) are considered as possible detector choices. We propose to use ^{18}Ne and ^6He as source ions for ν_e and $\bar{\nu}_e$ beams respectively. The maximum Lorentz boost factor, γ , available for these ions using the Tevatron are $\gamma_{\text{Ne}} = 585$ and $\gamma_{\text{He}} = 350$. This particular set-up provides the opportunity to probe the first oscillation maximum using ν_e beam and the second oscillation maximum using the $\bar{\nu}_e$ beam which helps to evade some parameter degeneracies. The resulting physics sensitivities for θ_{13} , CP violation and the mass hierarchy are compared to those of a conventional superbeam from FNAL to DUSEL.

*Electronic address: sanjib.at.vt.edu

†Electronic address: pahuber.at.vt.edu

1. INTRODUCTION

The discovery of neutrino mass is one of the first clear cases of physics beyond the Standard Model. Neutrino oscillation is now firmly established as the leading mechanism for flavor changes in neutrinos [1–7]. This has triggered substantial interest in precision measurements of neutrino properties, with a special emphasis on oscillation experiments. A new generation of long baseline [8, 9] and reactor [10] experiments is currently trying to measure θ_{13} . This is considered to be the first step to a large scale experimental program of long baseline neutrino experiments which aim at determining the neutrino mass ordering and to study leptonic CP violation, see *e.g.* [11, 12]. Due to experimental constraints on the available neutrino flavors in both source and detector, the most promising oscillation channels are the ones where a muon (anti-)neutrino oscillates into an electron (anti-)neutrino or *vice versa*. In spite of using both neutrinos and anti-neutrinos, a serious problem with all long baseline experiments involving these channels, arises from discrete degeneracies which manifest themselves in three forms: the $(\theta_{13}, \delta_{\text{CP}})$ intrinsic degeneracy [13], the $(\text{sgn}(\Delta m_{31}^2), \delta_{\text{CP}})$ degeneracy [14], and the $(\theta_{23}, \pi/2 - \theta_{23})$ degeneracy [15]. This leads to an eight-fold degeneracy [16], with several degenerate solutions in addition to the true one. The presence of these degenerate solutions can severely limit the sensitivity of an experiment.

In this paper, we will consider a beta-beam, as originally proposed in [17]: a flavor pure beam of electron (anti-)neutrinos from the beta decay of ions of short lived isotopes, which are accelerated to a Lorentz factor, $\gamma > 100$. This idea has attracted a large community and there is a vast literature on the many different options for such a facility [18–38]. We present a study of beta-beam facility at FNAL. A somewhat similar idea has been explored in [35]: there, however the emphasis was on possible synergies between the new facility and NO ν A. We, on the other hand, focus on a full fledged, stand-alone beta-beam. We will use ^{18}Ne (for ν_e) and ^6He (for $\bar{\nu}_e$) ions. The maximum Lorentz boost factors using the Tevatron are $\gamma_{\text{Ne}} = 585$ and $\gamma_{\text{He}} = 350$ which yield energy spectra which peak at 2.3 GeV and 1.4 GeV, respectively. Our detector is located at DUSEL [39–41] at a distance of $L \simeq 1300$ km from FNAL. We propose to use a 300 kt WC detector or a 50 kt LArTPC as a possible detector candidate. The first and second oscillation maxima for the FNAL - DUSEL baseline are at 2.5 GeV and 0.8 GeV for $\Delta m_{31}^2 = 2.4 \cdot 10^{-3} \text{ eV}^2$. Therefore, this set-up provides an unique opportunity to work at the first oscillation maximum using the ν_e beam and the peak energy of the $\bar{\nu}_e$ beam is very close to the second oscillation maximum.

The paper is organized as follows. We begin with a brief description of the FNAL based beta-beam facility in Section 2. In Section 3, we deal with the relevant oscillation probabilities. In the following section (Section 4) we describe the characteristics of the WC detector and the LArTPC; also, we introduce the superbeam which will be used for comparison. We also present the expected event rates for these two detectors. The details of our numerical technique and analysis procedure are presented in Section 5. In Section 6, we present our results and provide a summary.

2. FERMILAB BASED BETA-BEAM

The concept of a beta-beam was proposed in [17]: a pure, intense, collimated beam of electron neutrinos or their antiparticles from the beta-decay of completely ionized unstable

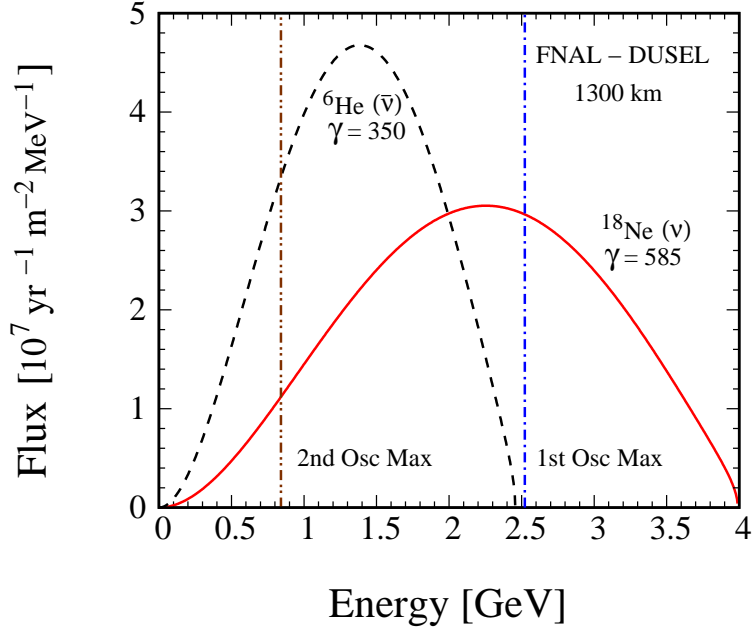


FIG. 1: The un-oscillated beta-beam flux spectrum arriving at a detector placed at DUSEL at a distance of 1300 km from FNAL. The red solid line shows the ν_e spectrum generated from ^{18}Ne with $\gamma = 585$. The black dashed curve depicts the $\bar{\nu}_e$ spectrum originated from ^6He with $\gamma = 350$. The blue dot-dashed and the brown double-dot-dashed vertical lines show the locations of first and second oscillation maximum for the FNAL -DUSEL baseline corresponding to $\Delta m_{31}^2 = 2.4 \cdot 10^{-3} \text{ eV}^2$.

radioactive ions circulating in a decay ring. The first stage in a beta-beam are protons with an energy of a few GeV which impinge a neutron spallation target. These neutrons, then interact in a secondary target to produce the desired unstable isotopes, in our case ^{18}Ne and ^6He (see, table I). Both are noble gases and, therefore can easily diffuse out of the secondary target, where they are collected, ionized and bunched. Now, they can be accelerated and be put into a storage ring with long straight sections. The decay of the highly boosted ions in the straight sections then yields an intense, well collimated, flavor pure electron (anti-)neutrino beam of known flux and spectrum, see *e.g.* [42, 43]. Feasibility of this proposal and its physics reach is being studied in great detail [19]. The set-up we propose will take full advantage of existing accelerator facilities at FNAL [35]. The main limitation is the maximum energy per nucleon the Tevatron can achieve. The maximum γ available for the ions considered here, using the Tevatron as accelerator, are $\gamma_{\text{Ne}} = 585$ and $\gamma_{\text{He}} = 350$. We have also studied the possibility to use ^8B and ^8Li . These two isotopes have much larger endpoint energies, of more than 10 MeV and thus would allow to have a peak energy for both neutrino and anti-neutrinos around the 1st oscillation maximum. However, since they would require a much lower γ , they would yield a considerably smaller neutrino flux. We have performed a full numerical study for these ions for the full range of available γ and found that their performance is always worse than for ^6He and ^{18}Ne . In a similar fashion, we have optimized the γ for ^6He and ^{18}Ne and the values chosen above represent the optimum in terms of physics sensitivities at the given baseline. Since, ion production requires a proton power of only a few 50 kW, the currently available proton intensities may

Ion	$t_{1/2}$ (s)	E_0 (MeV)	Total useful decays	γ (Tevatron)	Beam	$E_{\text{lab}}^{\text{peak}}$ (GeV)
${}^{18}_{10}\text{Ne}$	1.67	3.92	$5 \cdot (1.1 \cdot 10^{18})$	585	ν_e	2.3
${}^6_2\text{He}$	0.81	4.02	$5 \cdot (2.9 \cdot 10^{18})$	350	$\bar{\nu}_e$	1.4

TABLE I: The beta-decay parameters, half-life $t_{1/2}$ and electron total end-point energy E_0 are shown in the first two columns [44]. In the third column, we list the total number of useful ion decays considered in this work. The maximum γ available for these ions using the Tevatron are mentioned in column four. The peak energies of the ν_e and $\bar{\nu}_e$ spectrum in the lab frame are shown in the last column.

be sufficient. A new decay ring of about 14.7 km in circumference (assuming 5 T magnetic field and 36% useful decay fraction), however, needs to be built to store the ions.

While the shape of the beam spectrum depends on the end-point energy E_0 and the Lorentz boost γ of the parent ions, the flux normalization is controlled by the number of useful ion decays per year in one of the straight sections of the storage ring N_β . Table I depicts the relevant details of the properties of these ions and their considered luminosities and the choices of γ . We have assumed $1.1 \cdot 10^{18}$ (ν_e) and $2.9 \cdot 10^{18}$ ($\bar{\nu}_e$) useful ion decays per year for ${}^{18}\text{Ne}$ and ${}^6\text{He}$ ions respectively [45].

Figure 1 shows the un-oscillated beta-beam flux reaching at a detector placed at the DUSEL site at a distance of 1300 km from FNAL. We see from this figure that the ν_e ($\bar{\nu}_e$) spectrum peaks at 2.3(1.4) GeV. The first and second oscillation maxima for the FNAL - DUSEL baseline are at 2.5 GeV and 0.8 GeV for $\Delta m_{31}^2 = 2.4 \cdot 10^{-3} \text{ eV}^2$. Therefore, the ν_e spectrum is well suited for the first oscillation maximum whereas the $\bar{\nu}_e$ flux is sensitive to the second oscillation maximum.

3. THE $P_{e\mu}$ OSCILLATION CHANNEL

The simulation work presented in this paper is based on the full three flavor neutrino oscillation probabilities in matter, using the preliminary reference Earth model for the Earth matter density [46]. However, to explain the nature of neutrino oscillations as a function of baseline and/or neutrino energy, it is crucial to use approximate analytic expression for $P_{e\mu}$ in matter [47–49], keeping terms only up to second order in the small quantities θ_{13} and $\alpha \equiv \Delta m_{21}^2 / \Delta m_{31}^2$ [50, 51]

$$\begin{aligned}
P_{e\mu} \simeq & \underbrace{\sin^2 \theta_{23} \sin^2 2\theta_{13} \frac{\sin^2[(1 - \hat{A})\Delta]}{(1 - \hat{A})^2} + \alpha^2 \cos^2 \theta_{23} \sin^2 2\theta_{12} \frac{\sin^2(\hat{A}\Delta)}{\hat{A}^2}}_{T_0} \\
& \pm \underbrace{\alpha \sin 2\theta_{13} \sin 2\theta_{12} \sin 2\theta_{23} \sin(\Delta) \frac{\sin(\hat{A}\Delta)}{\hat{A}} \frac{\sin[(1 - \hat{A})\Delta]}{(1 - \hat{A})}}_{T_-} \sin \delta_{\text{CP}}
\end{aligned}$$

Detector Characteristics	WC (Both μ^\pm & e^\pm) (Only QE Sample)	LArTPC (Both μ^\pm & e^\pm) (QE & IE Sample)
Fiducial Mass	300 kt	50 kt
Energy Threshold	WC: A/WC: B	0.2 GeV
Detection Efficiency (ϵ)	80%	80%
Energy Resolution (δE) (GeV)	$0.085+0.05\sqrt{E/\text{GeV}}$	$0.085+0.05\sqrt{E/\text{GeV}}$ for QE Sample $0.085+0.2\sqrt{E/\text{GeV}}$ for IE Sample
Bin Size	0.2 GeV	0.2 GeV
Background Rejection	WC: A/WC: B	$10^{-3}/10^{-4}$
Signal error (syst.)	2.5%	2.5%
Background error (syst.)	5%	5%

TABLE II: Detector characteristics used in the simulations. The bin size is kept fixed, while the number of bins is varied according to the maximum energy. We use two different simulation methods (WC: A & WC: B) to treat the backgrounds in WC detector. Details can be found in Section 4.

$$+ \underbrace{\alpha \sin 2\theta_{13} \sin 2\theta_{12} \sin 2\theta_{23} \cos(\Delta) \frac{\sin(\hat{A}\Delta)}{\hat{A}} \frac{\sin[(1-\hat{A})\Delta]}{(1-\hat{A})}}_{T_+} \cos \delta_{\text{CP}}, \quad (1)$$

where

$$\Delta \equiv \frac{\Delta m_{31}^2 L}{4E}, \quad \hat{A} \equiv \frac{A}{\Delta m_{31}^2}, \quad A = \pm 2\sqrt{2}G_F N_e E. \quad (2)$$

Here, A is the matter potential, expressed in terms of the electron density N_e and the (anti)neutrino energy E ; ‘+’ sign refers to neutrinos whereas ‘-’ to anti-neutrinos.

4. EVENT RATES AT THE DETECTORS AT DUSEL

Currently, two technologies for large underground neutrino detection are considered for DUSEL: either a 300 kt WC detector or a 50 kt LArTPC [39, 41]. In the following, we will describe their different properties as far as needed for this work and we summarize them in table II. We do not consider backgrounds due to atmospheric neutrinos for either detector. The timing information of the ion bunches turns out to be sufficient to reduce these backgrounds down to an insignificant level, see, *e.g.* the appendix of [26].

A. Water Cherenkov Detector

The water Cherenkov technology is well understood on a large scale [3] and has demonstrated its excellent capability to distinguish muons from electrons. In a beta-beam, the

appearance signal are muons from charged current ν_μ interactions; this has the advantage that they are easier to distinguish from neutral current (NC) events than electrons. Nonetheless, NC events, in particular those involving one or several neutral pions, are problematic and they are the major source of background. Above the pion production threshold, the background level depends on how well neutral pions can be identified and distinguished from muons. Here, we consider only quasi-elastic (QE) charged current events for the appearance signal. We assume 80% detection efficiency, ϵ , for both muon and electron QE events (see table II). More precisely, we should consider single ring events, *i.e.* for signal events, these events are characterized by only one charged particle being above Cherenkov threshold. For the NC background, this signature can be mimicked if the two photons from a π^0 decay are so close that the subsequent Cherenkov rings cannot be separated. This is more likely to happen for energetic π^0 since the opening angle between the two photons is determined by the Lorentz γ of the parent particle. Note, that identifying the quasi-elastic events with the single ring events is a reasonable approximation for the signal events. For the spectral analysis, we include Fermi-motion by term of a constant width of 85 MeV [8] in the resolution function. The energy resolution for the muon and electron is 5% of $\sqrt{E/\text{GeV}}$ and the resulting width of the Gaussian energy resolution function is the sum of both terms.

As mentioned previously, for NC background events there is no simple, physically accurate approximation to their rate. Therefore, we will resort to two different phenomenological parametrization. The first one, method A, is based on an actual Super-K based Monte Carlo simulation, whereas the second one, method B, assumes an energy independent NC rejection efficiency.

In method A, labeled as ‘WC: A’, we follow the results presented in [52] where the authors study the performance of a water Cherenkov detector in a beta-beam using the current simulation and analysis tools developed for the Super-Kamiokande experiment. Results are derived for a baseline of 700 (130) km and taking $\gamma = 350$ (100) for both ^{18}Ne and ^6He ions. As far as the background is concerned, the main outcome of this study is, that the major background events in the search for ν_μ appearance signal are indeed NC interactions involving pions. In a NC interaction, the outgoing neutrino carries a large and generally unknown fraction of the incoming neutrino energy. Therefore, those NC events which pass the single ring selection criteria tend to be reconstructed with an energy much lower than the true, incoming neutrino energy. It turns out, that, because of this, it is possible to maximize the signal to background ratio by imposing a cut in reconstructed energy. Unfortunately, in reference [52] only results for $\gamma = 100$ and $\gamma = 350$ are presented, therefore we will extrapolate these results to the values of γ of interest for this work. We assume that the average energy of a mis-reconstructed NC event, *i.e.* the ones which pass the muon single ring selection, is proportional to the incoming, true neutrino energy *and* that the proportionality constant does not change appreciable over the energy range considered. This intuition is inspired by the form of the differential NC cross section $d\sigma/dy$, where $y = E_q/E$, with E being the energy of the incoming neutrino and E_q the energy transferred to the target. Therefore, we will assume that the energy cut which effectively removes the NC background is proportional to the average true neutrino event energy $\langle E \rangle_{NC}$

$$\langle E \rangle_{NC} = \frac{\int \phi(E) E \sigma_{NC}(E) dE}{\int \phi(E) \sigma_{NC}(E) dE} , \quad (3)$$

where $\phi(E)$ is the (anti-)neutrino beta-beam flux produced at the source and $\sigma_{NC}(E)$ is the NC cross-section. We define a so called threshold factor, T_f which is different for neutrinos and anti-neutrinos, but independent of γ

$$E_T = T_f \langle E \rangle_{NC}, \quad (4)$$

with E_T being the threshold in reconstructed energy above which there is no NC background left. It is straightforward to compute $\langle E \rangle_{NC} = 1.57$ (1.69) GeV for ^{18}Ne (^6He) ions with $\gamma = 350$. From reference [52], we find that $E_T = 1$ GeV is sufficient for $\gamma = 350$ to eliminate all the backgrounds for both neutrinos and anti-neutrinos. Using equation 4, we obtain

$$T_f = 0.64 \text{ (0.59)} \quad \text{for } ^{18}\text{Ne} \text{ (} ^6\text{He)}. \quad (5)$$

Reference [52] provides also results for $\gamma = 100$ and we can use these to test our assumption that T_f is independent of γ . For $\gamma = 100$, we have $\langle E \rangle_{NC} = 0.48$ (0.5) GeV for ^{18}Ne (^6He) ions. Now using the values of T_f given by equation 5, we get $E_T = 0.3$ GeV for both ^{18}Ne & ^6He ions which matches exactly with the value of E_T obtained in [52] for $\gamma = 100$. This nicely demonstrates that the parametrization in terms of T_f and $\langle E \rangle_{NC}$ works over a reasonably large range of energies. With $\gamma = 585$ for ^{18}Ne ions we have $\langle E \rangle_{NC} = 2.62$ GeV. Now using the value $T_f = 0.64$ given in equation 5, we obtain $E_T = 1.7$ GeV. Summarizing, for method A, we use a threshold energy of 1.7 (1) GeV for $\gamma = 585$ (350) for both neutrinos and anti-neutrinos and assume that there is no NC background above E_T .

In the second method, labeled as ‘WC: B’, we take a threshold of 0.2 GeV, which is close the production threshold for muons and take the background to be a 10^{-3} of the NC current rate. The shape of this background is identical to $\phi(E)\sigma_{NC}(E)$ and for simplicity, we use the same energy resolution function to smear the NC backgrounds that we use for QE signal events.

The impact of these two different simulation methods (WC: A & WC: B) is quite different while we calculate the sensitivity and we will discuss it in detail in Section 6.

For our superbeam result which are shown for comparison only, we use the identical setup as in Section 10 of [41].

B. Liquid Argon Time Projection Chamber

A LArTPC works due to the fact, that by applying an electric field, free electrons created by the passage of an ionizing particle can be drifted over large distances, $\mathcal{O}(m)$, without distortion. This allows, to obtain three projections of the particle track by just reading out the surface of the volume. For this reason, it seems feasible to build very large LArTPCs at a reasonable cost. The three projections of the track can be used to reconstruct the three dimensional path of the particle with an accuracy of a few mm. The currently largest LArTPC ever built, is the ICARUS T600 module [53] with a mass of 600 t. It is recognized that scaling T600 by at least two orders of magnitude requires considerable R&D.

Since this technology is still in its R&D phase, much less knowledge regarding its performance exists. Thus, what we present here, are essentially educated guesses [54]. We divide the signal event into samples of QE and inelastic (IE) events because energy reconstruction

works quite differently for these two event classes¹. For QE events there are only very few tracks, typically the muon and the proton, thus it is feasible to perform a full kinematic analysis. Therefore, QE events will have a rather good energy resolution. IE events, on the other hand, will produce a large number of tracks, which the detector will not be able to separate and reconstruct individually. Most likely, only the muon track and a shower-like object can be identified, while the muon still is reconstructed quite well, only summary information will be available for the shower, *e.g.* total charge. Thus, the shower energy resolution will be much worse than the muon resolution. Therefore, we will use two different energy resolution functions for QE and IE events [54]

$$\delta E_{QE}(E) = \left(0.085 + 0.05\sqrt{E/\text{GeV}}\right) \text{ GeV} \quad \text{for QE}, \quad (6)$$

$$\delta E_{IE}(E) = \left(0.085 + 0.2\sqrt{E/\text{GeV}}\right) \text{ GeV} \quad \text{for IE}. \quad (7)$$

We use 80% detection efficiency, ϵ , for both muon and electron QE and IE events (see table II). We calculate the sensitivity using two different values, 10^{-3} and 10^{-4} , for the background rejection factor. The present status of the simulation study of the LArTPC at the DUSEL site can be found in Section 10 of [41].

As we divide the signal events into two parts, we divide the NC backgrounds into two parts as well. At a given energy E , the NC backgrounds, which are relevant to estimate the sensitivity, are calculated in the following way

$$(\text{NC})_{total}^E = \underbrace{(\text{NC})_{total}^E \times \frac{\sigma_{QE}}{\sigma_{total}}}_{(\text{NC})_{QE}^E} + \underbrace{(\text{NC})_{total}^E \times \frac{\sigma_{IE}}{\sigma_{total}}}_{(\text{NC})_{IE}^E}, \quad (8)$$

where $(\text{NC})_{QE}^E$ and $(\text{NC})_{IE}^E$ are the NC backgrounds² applicable for QE and IE events respectively. σ_{QE} , σ_{IE} and σ_{total} are the relevant neutrino interaction cross-sections.

C. Event Rates

The number of (anti-)muon events³ in the i -th energy bin in the detector is given by

$$N_i = \frac{T n_n \epsilon}{4\pi L^2} \int_0^{E_{\max}} dE \int_{E_{A_i}^{\min}}^{E_{A_i}^{\max}} dE_A \phi(E) \sigma_{\nu\mu}(E) R(E, E_A) P_{e\mu}(E), \quad (9)$$

¹ We assume that QE and IE events are fully uncorrelated with each other and that they can be cleanly separated.

² The $(\text{NC})_{QE}^E$ and $(\text{NC})_{IE}^E$ backgrounds are smeared using the same energy resolution function that we use for QE and IE signal events respectively. Again, this choice is justified more by its apparent simplicity than by its realism.

³ In principle, both detectors, also are sensitive to electron (positron) events. The number of electron events can be calculated using equation 9, by making appropriate changes to the oscillation probability and cross-sections. However, as was noted in [25], electron disappearance has hardly any sensitivity to θ_{13} and mass ordering at short baselines like the one under discussion. Also, it does not depend on δ_{CP} .

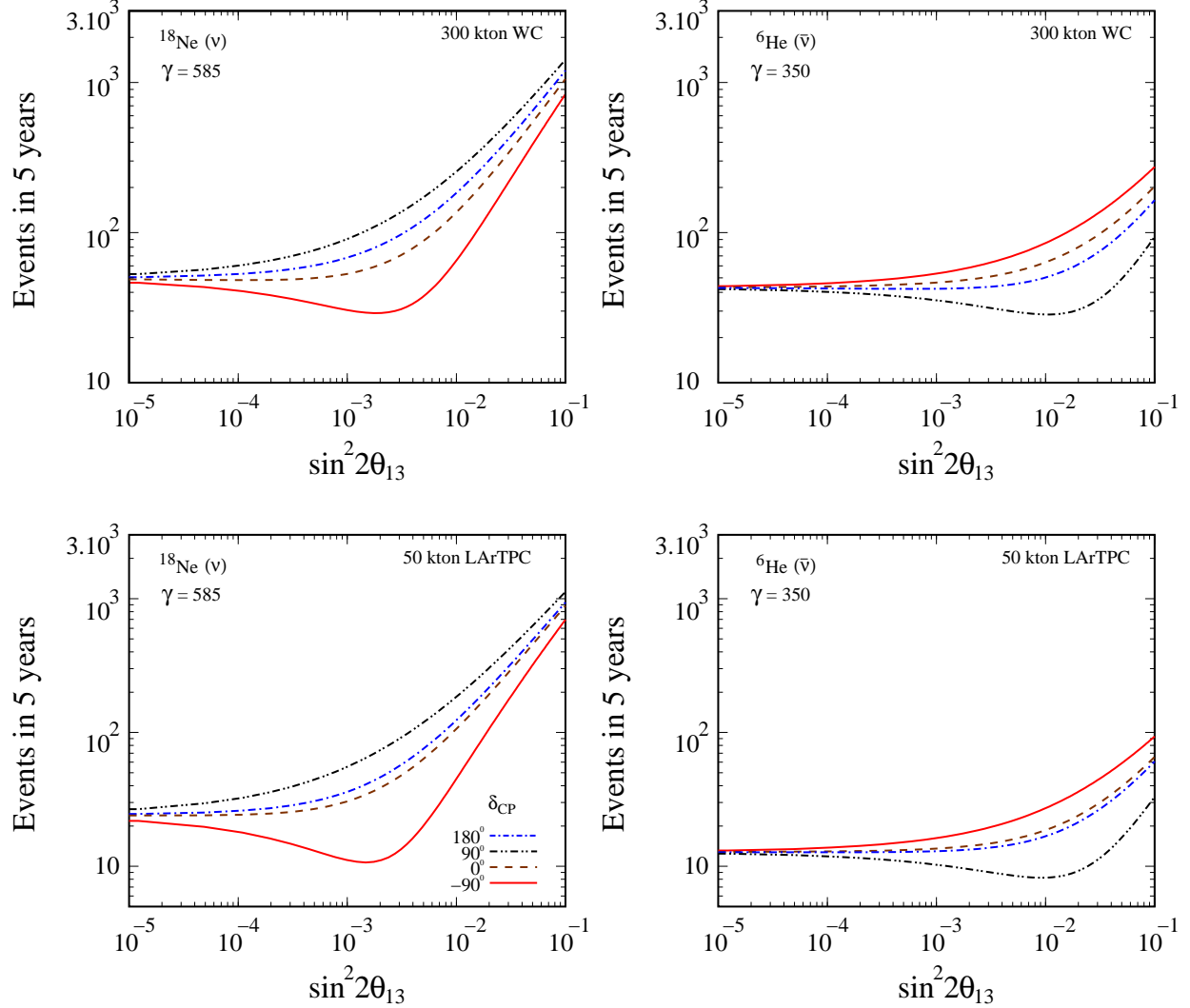


FIG. 2: Total event rates in five years as a function of $\sin^2 2\theta_{13}$ in the FNAL - DUSEL set-up for ^{18}Ne (ν_e) with $\gamma = 585$ and ^6He ($\bar{\nu}_e$) with $\gamma = 350$ are shown. The upper panels are for a 300 kt WC detector, while the lower ones are for a 50 kt LArTPC. Results are depicted for four different values of δ_{CP} : -90° , 0° , 90° , and 180° . Normal hierarchy has been assumed. For all other oscillation parameters we use the values given in equation 10.

where T is the total running time, n_n is the number of target nucleons in the detector, ϵ is the detector efficiency and $R(E, E_A)$ is the Gaussian energy resolution function of the detector. For muon (anti-muon) events, σ_{ν_μ} is the neutrino (anti-neutrino) interaction cross-section. The quantities E and E_A are the true and reconstructed (anti-)neutrino energies respectively and L is the baseline.

We simulate the signal event spectrum using equation 9 for our assumed true⁴ values for

⁴ We distinguish between the “true” values of the oscillation parameters, which are used to compute the data, and their fitted values. Throughout this paper we denote the true value of a parameter by putting “(true)” after the symbol for the parameter.

the set of oscillation parameters as given in equation 10. The left-hand panels of figure 2 portray the number of neutrino events expected at DUSEL from five years exposure of the ^{18}Ne beta-beam from FNAL with $\gamma = 585$ while the right-hand panels show the anti-neutrino events from five years run of the ^6He beta-beam with $\gamma = 350$. Results are presented as a function of $\sin^2 2\theta_{13}$ for four different values of δ_{CP} : -90° , 0° , 90° , and 180° with normal mass hierarchy. The upper panels are for a 300 kt WC detector, while the lower panels are for a 50 kt LArTPC. The number of events (both for ^{18}Ne and ^6He) varies in a wide range with the choice of δ_{CP} . Out of the four different choices of δ_{CP} , the maximum (minimum) number of events for neutrinos is obtained with 90° (-90°) irrespective of the choice of $\sin^2 2\theta_{13}$. For anti-neutrinos, the same is true with $\delta_{\text{CP}} \rightarrow -\delta_{\text{CP}}$. We can explain this fact with the help of equation 1. At the FNAL - DUSEL baseline, matter effects are small and hence $\hat{A} \ll 1$ in equation 2. The oscillation probabilities can be expressed as $P_{e\mu} \simeq T_0 + T_- \sin \delta_{\text{CP}} + T_+ \cos \delta_{\text{CP}}$ and $P_{\bar{e}\bar{\mu}} \simeq T_0 - T_- \sin \delta_{\text{CP}} + T_+ \cos \delta_{\text{CP}}$, where T_0, T_\pm are independent of δ_{CP} , whence the symmetry is manifest. For most of the energies T_- is positive assuming normal hierarchy. Now for $\delta_{\text{CP}} = 90^\circ$ (-90°) the term $T_- \sin \delta_{\text{CP}}$ gives a positive (negative) contribution towards the probability for neutrinos. The opposite is true for anti-neutrinos. The behavior of the number of events with $\sin^2 2\theta_{13}$ is also understandable. As we increase the value of $\sin^2 2\theta_{13}$ from a near-zero value, the 2nd and 3rd terms in equation 1, which are linear in $\sin 2\theta_{13}$ and are dependent on δ_{CP} , begin to contribute at first. Beyond a certain value of $\sin^2 2\theta_{13}$, the first term, which does not depend on δ_{CP} , takes over leading to the rise for all curves, but the relative size of CP effects decreases. This is the reason, why the discovery of leptonic CP violation does not become any easy task at large $\sin^2 2\theta_{13}$.

As far as the total number of neutrino events is concerned, the performance of the different detectors is less different than indicated by a factor of six difference in the detector masses (see the upper and lower left panels of figure 2). The reason is, that for the WC detector we consider only QE events but for the LArTPC we take into account both QE and IE events. At the same time the IE cross section is larger than the QE one at the relevant energies, see figure 1.

D. Reference set-up

In order to compare the beta-beam set-up to alternative possibilities at FNAL, we introduce the wide-band beam concept. This project has been studied in detail in [41, 55]. Here, a conventional neutrino beam will be sent from FNAL to a 300 kt WC in DUSEL. This beam has a spectrum wide enough to cover the first and second oscillation maximum and therefore can resolve most degeneracies. We use the same implementation as in [55], with exception of the beam spectrum, which has been updated to correctly represent the beam which would be produced at FNAL [56]. Also, the beam intensity now corresponds to 1.2 MW, this is the maximum beam power which can be achieved at FNAL without Project X [57]. The resulting physics sensitivities have been computed using GLOBES [58] and are shown as green shaded regions in figure 4.

5. THE NUMERICAL TECHNIQUE

For all calculations we use as central (true) values

$$\begin{aligned} |\Delta m_{31}^2| &= 2.4 \cdot 10^{-3} \text{ eV}^2 \pm 5\%, & \sin^2 2\theta_{23} &= 1.0 \pm 1\% \\ \Delta m_{21}^2 &= 7.6 \cdot 10^{-3} \text{ eV}^2 \pm 2\%, & \sin^2 \theta_{12} &= 0.32 \pm 6\%. \end{aligned} \quad (10)$$

In all fits, these parameters are allowed to vary within the stated 1σ intervals. The central values are the current best fit values [59]; also the errors on the solar parameters are taken from [59]. The errors on the atmospheric parameters correspond to the result which are expected from T2K and NO ν A [60].

Here, we describe in detail the numerical procedure adopted to calculate the discovery potential of the FNAL - DUSEL beta-beam set-up. For our statistical analysis we use the following χ^2 functions for WC detector and LArTPC

$$\begin{aligned} (\chi_{total}^2)_{\text{WC}} &= \chi_{(\nu_e \rightarrow \nu_\mu)_{\text{QE}}}^2 + \chi_{(\bar{\nu}_e \rightarrow \bar{\nu}_\mu)_{\text{QE}}}^2 \\ &+ \chi_{(\nu_e \rightarrow \nu_e)_{\text{QE}}}^2 + \chi_{(\bar{\nu}_e \rightarrow \bar{\nu}_e)_{\text{QE}}}^2 \\ &+ \chi_{\text{prior}}^2 \end{aligned} \quad (11)$$

and

$$\begin{aligned} (\chi_{total}^2)_{\text{LArTPC}} &= \chi_{(\nu_e \rightarrow \nu_\mu)_{\text{QE}}}^2 + \chi_{(\nu_e \rightarrow \nu_\mu)_{\text{IE}}}^2 + \chi_{(\bar{\nu}_e \rightarrow \bar{\nu}_\mu)_{\text{QE}}}^2 + \chi_{(\bar{\nu}_e \rightarrow \bar{\nu}_\mu)_{\text{IE}}}^2 \\ &+ \chi_{(\nu_e \rightarrow \nu_e)_{\text{QE}}}^2 + \chi_{(\nu_e \rightarrow \nu_e)_{\text{IE}}}^2 + \chi_{(\bar{\nu}_e \rightarrow \bar{\nu}_e)_{\text{QE}}}^2 + \chi_{(\bar{\nu}_e \rightarrow \bar{\nu}_e)_{\text{IE}}}^2 \\ &+ \chi_{\text{prior}}^2. \end{aligned} \quad (12)$$

The $\chi_{(\nu_e \rightarrow \nu_\mu)_{\text{QE}}}^2$ is given by

$$\chi_{(\nu_e \rightarrow \nu_\mu)_{\text{QE}}}^2 = \min_{\xi_s, \xi_b} \left[2 \sum_{i=1}^n (\tilde{y}_i - x_i - x_i \ln \frac{\tilde{y}_i}{x_i}) + \xi_s^2 + \xi_b^2 \right], \quad (13)$$

where n is the total number of bins and

$$\tilde{y}_i(\{\omega\}, \{\xi_s, \xi_b\}) = N_i^{\text{th}}(\{\omega\}) [1 + \pi^s \xi_s] + N_i^b [1 + \pi^b \xi_b]. \quad (14)$$

Above, $N_i^{\text{th}}(\{\omega\})$ is the predicted number of QE events (calculated using equation 9) in the i -th energy bin for a set of oscillation parameters ω and N_i^b are the number of background events in bin i . The quantities π^s and π^b in equation 14 are the systematical errors on signals and backgrounds respectively. We consider $\pi^s = 2.5\%$ and $\pi^b = 5\%$ (see table II). The quantities ξ_s and ξ_b are the pulls due to the systematical error on signal and background respectively. The data from equation 13 enters through the variable $x_i = N_i^{\text{ex}} + N_i^b$, where N_i^{ex} is the number of observed QE signal events in the detector and N_i^b is the background, as mentioned earlier. We simulate the QE signal event spectrum using equation 9 for our assumed true values for the set of oscillation parameters given in equation 10. We consider all the values of $\sin^2 2\theta_{13}$ (true) and δ_{CP} (true) in their allowed range and assume NH as true hierarchy. In a similar way, we estimate the contributions towards χ_{total}^2 coming from other oscillation channels and event types (for both neutrino and anti-neutrino modes). In

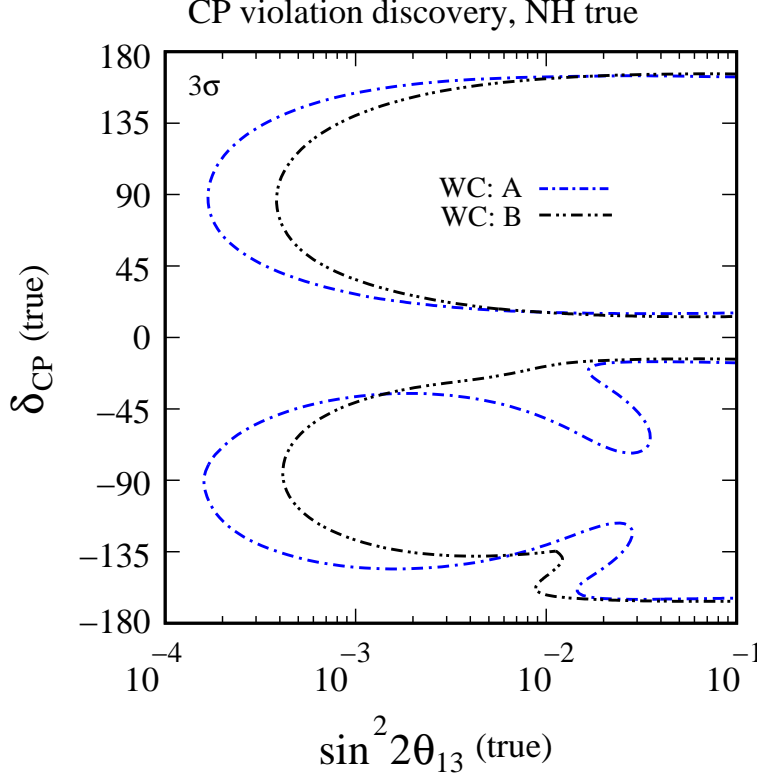


FIG. 3: CP violation discovery potential of beta-beam at 730 km as range of δ_{CP} (true) as a function of the $\sin^2 2\theta_{13}$ (true) assuming normal hierarchy as true hierarchy at the 1 d.o.f. 3σ C.L. Here we take $\gamma = 350$ for both ^{18}Ne & ^6He ions. The results are shown for 300 kt WC detector assuming two different simulation methods. See the text for details.

our χ^2 fit we marginalize over *all* oscillation parameters and as well as the neutrino mass ordering, as applicable. We perform this by allowing all of these to vary freely in the fit and picking the smallest value of the χ^2 function. However, we assume that some of these parameters which are poorly constrained by this experimental set-up, will be measured better from other experiments. Therefore, we impose a prior, or external constraint, on these parameters through χ^2_{prior} , given by

$$\begin{aligned} \chi^2_{\text{prior}} = & \left(\frac{|\Delta m_{31}^2| - |\Delta m_{31}^2(\text{true})|}{\sigma(|\Delta m_{31}^2|)} \right)^2 + \left(\frac{\sin^2 2\theta_{23} - \sin^2 2\theta_{23}(\text{true})}{\sigma(\sin^2 2\theta_{23})} \right)^2 \\ & + \left(\frac{\Delta m_{21}^2 - \Delta m_{21}^2(\text{true})}{\sigma(\Delta m_{21}^2)} \right)^2 + \left(\frac{\sin^2 \theta_{12} - \sin^2 \theta_{12}(\text{true})}{\sigma(\sin^2 \theta_{12})} \right)^2. \end{aligned} \quad (15)$$

where the 1σ errors on these, are given in equation 10. We minimize the χ^2_{total} using the same procedure as it was described in the appendix of [23].

6. RESULTS & SUMMARY

We evaluate the physics reach of the FNAL - DUSEL beta-beam set-up in terms of its discovery potentials for $\sin^2 2\theta_{13}$, CP violation and the mass hierarchy. These discovery po-

tentials quantify for any given $\sin^2 2\theta_{13}$ (true) for which range of possible values of δ_{CP} (true) the corresponding quantity will be discovered or measured at the chosen confidence level. The discovery reach for $\sin^2 2\theta_{13}$ is defined by the minimum value of $\sin^2 2\theta_{13}$ (true) which allows us to rule out $\sin^2 2\theta_{13} = 0$ in the fit. The CP violation discovery potential is defined as the range of δ_{CP} (true) as a function of $\sin^2 2\theta_{13}$ (true) for which one can use the data to exclude the CP conserving solutions $\delta_{\text{CP}} = 0^\circ$ and $\delta_{\text{CP}} = 180^\circ$. The mass hierarchy discovery reach is the limiting value of $\sin^2 2\theta_{13}$ (true) for which the wrong hierarchy can be excluded.

Before we present our results for FNAL - DUSEL beta-beam set-up, we would like to discuss the CP violation discovery potential of beta-beam using a 300 kt WC detector at 730 km taking $\gamma = 350$ for both ^{18}Ne & ^6He ions (see figure 3). This setup has already been considered in the literature and has been shown provide high performance [33]. The first and second oscillation maxima for 730 km baseline are at 1.4 GeV and 0.5 GeV for $\Delta m_{31}^2 = 2.4 \cdot 10^{-3} \text{ eV}^2$. At this baseline, both the ν_e and the $\bar{\nu}_e$ beam peak at the first oscillation maximum for $\gamma = 350$. Also for this setup, we use two methods to treat the NC background in the water Cherenkov detector as described in section 4 A. For method A, we have a threshold energy of 1 GeV for both ^{18}Ne and ^6He ions and assume no backgrounds above the threshold. Since there is no background left above 1 GeV, it is possible to probe CP violation at very small values of $\sin^2 2\theta_{13}$ (true) as depicted by the dash-dotted blue line of figure 3. The major drawback of this method is that we do not have any access to the second oscillation maximum. Therefore, the $(\text{sgn}(\Delta m_{31}^2), \delta_{\text{CP}})$ degeneracy for large values of $\sin^2 2\theta_{13}$ (true) is fully developed; as a result there is a sizable gap in sensitivity around $\sin^2 2\theta_{13}$ (true) = $3 \cdot 10^{-2}$. This effect has been described in [61] and has been termed π -transit.

For method B, shown as dash-double-dotted black line in figure 3, where the threshold is 0.2 GeV and a background rejection factor of 10^{-3} is used for both the ions. Although the total backgrounds are higher, the second oscillation maximum can be used, nonetheless. Therefore, the effects of π -transit are mitigated for most of the parameter space, *i.e.* the sensitivity at large θ_{13} has essentially no gaps. The higher backgrounds result, however, in a reduced reach for small values of θ_{13} . This concludes our comparison with previous results.

Our results are summarized in figure 4, where the physics sensitivities for $\sin^2 2\theta_{13}$ (left panel), CP violation (middle panel), and for the mass hierarchy (right panel) are shown for a baseline of 1300 km. Results are shown at the 3σ confidence level for one degree of freedom. The various line styles are for the different detector options and background levels as given in the legend. The green shaded areas are the corresponding results for a conventional superbeam from FNAL to DUSEL using a 300 kt WC detector as described in detail in [55].

For the WC detector, we observe a distinct difference in sensitivities between the two different schemes to include background (black, dash-double-dotted line and blue, dash-dotted line). Clearly, using a hard energy cut (WC: A, blue, dash-dotted line), which eliminates essentially all background and all information from the second oscillation maximum, performs better than WC: B (black, dash-double-dotted line). The only exception is found for the CP violation reach around $\sin^2 2\theta_{13} = 5 \cdot 10^{-3}$ for a CP phase of approximately -120° . The reason, is the loss in information from the second oscillation maximum. Taking WC: A as our benchmark case, we find that a beta beam would result in about one order of magnitude improvement over a superbeam for all three measurements for at least one half of the CP phases. The performance of a 50 kt LArTPC is rather similar to the one of a six times larger

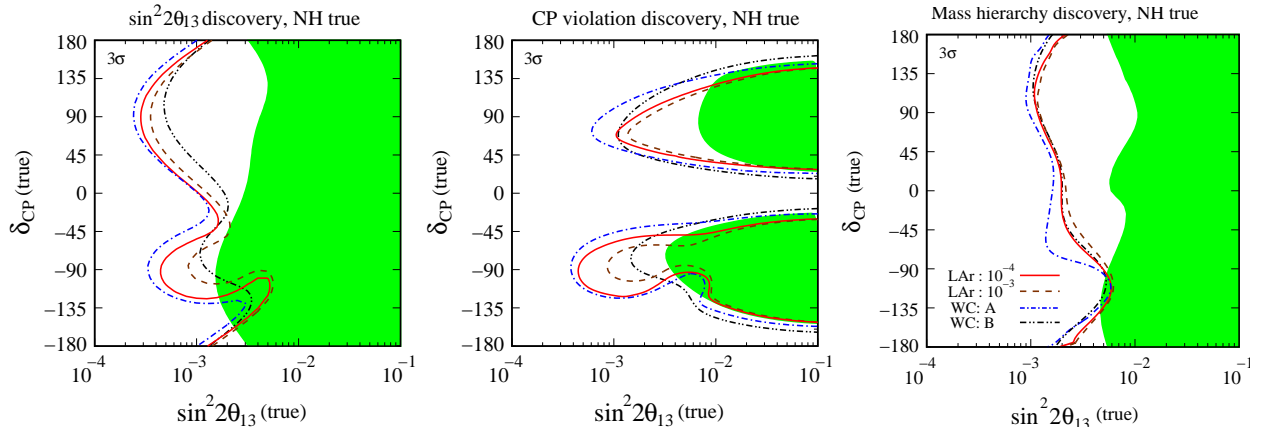


FIG. 4: Performance of FNAL - DUSEL beta-beam set-up at the 1 d.o.f. 3σ C.L. in addressing $\sin^2 2\theta_{13}$, CP violation, and mass hierarchy discovery potential as range of $\delta_{CP}(\text{true})$ as a function of the $\sin^2 2\theta_{13}(\text{true})$ assuming normal hierarchy as true hierarchy. The results are shown for 300 kt WC detector (assuming the simulation methods WC: A & WC: B. See Section 4 for details) and 50 kt LArTPC (assuming the background rejection factor of 10^{-3} and 10^{-4}). The green shaded regions show the sensitivity of a wide band beam using the WC detector, as defined in detail in section 4 D.

WC detector using background scheme B.

In comparison to the superbeam, shown as green shaded regions and described in section 4 D, we see that using the same 300 kt WC detector the gain from using a beta-beam is obvious and most pronounced for $0 < \delta_{CP} < 180^\circ$. This statement holds also for the use of a six times smaller 50 kt LArTPC. It is left to the judgement of the reader, whether the physics gain from a beta beam is commensurate to the effort of building a decay ring and of running the Tevatron for another decade. We also have shown that, given the performance parameters of the Tevatron, a baseline of around 730 km would provide a much more compelling physics gain. However, this baseline violates the boundary condition of locating the far detector at DUSEL. In summary, while a beta beam is a very interesting option to pursue high precision neutrino physics, especially the search for CP violation, it seems not to fit very well with existing and planned infrastructure in the US.

Acknowledgments

We would like to thank J. Link and D. Mohapatra for useful discussions. In particular we thank M. Mezzetto for detailed information on backgrounds in a Water Cherenkov detector. We acknowledge support from the U.S. Department of Energy under award number DE-SC0003915.

-
- [1] B. T. Cleveland *et al.*, *Astrophys. J.* **496**, 505 (1998); J. N. Abdurashitov *et al.* [SAGE Collaboration], *J. Exp. Theor. Phys.* **95**, 181 (2002)[*Zh. Eksp. Teor. Fiz.* **122**, 211 (2002)]; W. Hampel *et al.* [GALLEX Collaboration], *Phys. Lett. B* **447**, 127 (1999); S. Fukuda *et al.*

- [Super-Kamiokande Collaboration], Phys. Lett. B **539**, 179 (2002); B. Aharmim *et al.* [SNO Collaboration], Phys. Rev. C **72**, 055502 (2005); C. Arpesella *et al.* [Borexino Collaboration], Phys. Lett. B **658**, 101 (2008).
- [2] T. Araki *et al.* [KamLAND Collaboration], Phys. Rev. Lett. **94**, 081801 (2005); S. Abe *et al.* [KamLAND Collaboration], arXiv:0801.4589 [hep-ex].
- [3] Y. Fukuda *et al.* [Super-Kamiokande Collaboration], Phys. Rev. Lett. **81**, 1562 (1998); Y. Ashie *et al.* [Super-Kamiokande Collaboration], Phys. Rev. D **71**, 112005 (2005).
- [4] M. Apollonio *et al.*, Eur. Phys. J. C **27**, 331 (2003).
- [5] E. Aliu *et al.* [K2K Collaboration], Phys. Rev. Lett. **94**, 081802 (2005).
- [6] D. G. Michael *et al.*, [MINOS Collaboration], arXiv:hep-ex/0607088.
- [7] M. C. Gonzalez-Garcia and M. Maltoni, Phys. Rept. **460**, 1 (2008); S. Choubey, arXiv:hep-ph/0509217; S. Goswami, Int. J. Mod. Phys. A **21**, 1901 (2006); A. Bandyopadhyay, S. Choubey, S. Goswami, S. T. Petcov and D. P. Roy, Phys. Lett. B **608**, 115 (2005); G. L. Fogli *et al.*, Prog. Part. Nucl. Phys. **57**, 742 (2006).
- [8] Y. Itow *et al.*, arXiv:hep-ex/0106019.
- [9] D. S. Ayres *et al.* [NOvA Collaboration], arXiv:hep-ex/0503053.
- [10] F. Ardellier *et al.*, arXiv:hep-ex/0405032; X. Guo *et al.* [Daya-Bay Collaboration], arXiv:hep-ex/0701029.
- [11] <http://www.hep.ph.ic.ac.uk/iss/>
- [12] A. Bandyopadhyay *et al.* [ISS Physics Working Group], arXiv:0710.4947 [hep-ph].
- [13] J. Burguet-Castell, M. B. Gavela, J. J. Gómez-Cadenas, P. Hernandez and O. Mena, Nucl. Phys. B **608**, 301 (2001).
- [14] H. Minakata and H. Nunokawa, JHEP **0110**, 001 (2001).
- [15] G. L. Fogli and E. Lisi, Phys. Rev. D **54**, 3667 (1996).
- [16] V. Barger, D. Marfatia and K. Whisnant, Phys. Rev. D **65**, 073023 (2002).
- [17] P. Zucchelli, Phys. Lett. B **532**, 166 (2002).
- [18] For a recent review see C. Volpe, J. Phys. G **34**, R1 (2007).
- [19] The book written by Mats Lindroos and Mauro Mezzetto: *BETA BEAMS* (World Scientific, July, 2009).
- [20] S. K. Agarwalla, arXiv:0908.4267 [hep-ph].
- [21] J. E. Campagne *et al.*, JHEP **0704**, 003 (2007).
- [22] S. K. Agarwalla, A. Raychaudhuri and A. Samanta, Phys. Lett. B **629**, 33 (2005); S. K. Agarwalla, S. Choubey and A. Raychaudhuri, Nucl. Phys. B **771**, 1 (2007).
- [23] S. K. Agarwalla, S. Choubey and A. Raychaudhuri, Nucl. Phys. B **798**, 124 (2008).
- [24] S. K. Agarwalla, S. Choubey, A. Raychaudhuri and W. Winter, JHEP **0806**, 090 (2008).
- [25] S. K. Agarwalla, S. Choubey, S. Goswami and A. Raychaudhuri, Phys. Rev. D **75**, 097302 (2007).
- [26] S. K. Agarwalla, S. Choubey and A. Raychaudhuri, Nucl. Phys. B **805**, 305 (2008).
- [27] R. Adhikari, S. K. Agarwalla and A. Raychaudhuri, Phys. Lett. B **642**, 111 (2006); S. K. Agarwalla, S. Rakshit and A. Raychaudhuri, Phys. Lett. B **647**, 380 (2007).
- [28] S. K. Agarwalla, P. Huber and J. M. Link, arXiv:0907.3145 [hep-ph].
- [29] M. Mezzetto, J. Phys. G **29**, 1771 (2003); M. Mezzetto, Nucl. Phys. Proc. Suppl. **143**, 309 (2005); M. Mezzetto, Nucl. Phys. Proc. Suppl. **155**, 214 (2006).
- [30] A. Donini, E. Fernandez-Martinez, P. Migliozzi, S. Rigolin and L. Scotto Lavina, Nucl. Phys.

- B **710**, 402 (2005).
- [31] A. Donini, E. Fernandez, P. Migliozi, S. Rigolin, L. Scotto Lavina, T. Tabarelli de Fatis and F. Terranova, arXiv:hep-ph/0511134; A. Donini, E. Fernandez-Martinez, P. Migliozi, S. Rigolin, L. Scotto Lavina, T. Tabarelli de Fatis and F. Terranova, Eur. Phys. J. C **48**, 787 (2006).
 - [32] P. Coloma, A. Donini, E. Fernandez-Martinez and J. Lopez-Pavon, JHEP **0805**, 050 (2008); S. Choubey, P. Coloma, A. Donini and E. Fernandez-Martinez, arXiv:0907.2379 [hep-ph].
 - [33] J. Burguet-Castell, D. Casper, E. Couce, J. J. Gómez-Cadenas and P. Hernandez, Nucl. Phys. B **725**, 306 (2005).
 - [34] J. Burguet-Castell, D. Casper, J. J. Gómez-Cadenas, P. Hernandez and F. Sanchez, Nucl. Phys. B **695**, 217 (2004).
 - [35] A. Jansson, O. Mena, S. J. Parke and N. Saoulidou, Phys. Rev. D **78**, 053002 (2008).
 - [36] P. Huber, M. Lindner, M. Rolinec and W. Winter, Phys. Rev. D **73**, 053002 (2006).
 - [37] A. Donini and E. Fernandez-Martinez, Phys. Lett. B **641**, 432 (2006).
 - [38] D. Meloni, O. Mena, C. Orme, S. Palomares-Ruiz and S. Pascoli, JHEP **0807**, 115 (2008).
 - [39] <http://www.lbl.gov/nsd/homestake/>
 - [40] S. Raby *et al.*, arXiv:0810.4551 [hep-ph].
 - [41] V. Barger *et al.*, arXiv:0705.4396 [hep-ph].
 - [42] M. Lindroos, arXiv:physics/0312042; M. Lindroos, Nucl. Phys. Proc. Suppl. **155**, 48 (2006).
 - [43] <http://beta-beam.web.cern.ch/beta%2Dbeam/>
 - [44] L. P. Ekstrom and R. B. Firestone, WWW Table of Radioactive Isotopes, database version 2/28/99 from URL <http://ie.lbl.gov/toi/>
 - [45] B. Autin, R. C. Fernow, S. Machida and D. A. Harris, J. Phys. G **29**, 1637 (2003); F. Terranova, A. Marotta, P. Migliozi and M. Spinetti, Eur. Phys. J. C **38**, 69 (2004).
 - [46] A. M. Dziewonski and D. L. Anderson, Phys. Earth Planet. Interiors **25**, 297 (1981); S. V. Panasyuk, Reference Earth Model (REM) webpage, <http://cfauves5.harvard.edu/lana/rem/index.html>.
 - [47] L. Wolfenstein, Phys. Rev. D **17**, 2369 (1978);
 - [48] S. P. Mikheev and A. Y. Smirnov, Sov. J. Nucl. Phys. **42**, 913 (1985) [Yad. Fiz. **42**, 1441 (1985)]; S. P. Mikheev and A. Y. Smirnov, Nuovo Cim. C **9**, 17 (1986).
 - [49] V. D. Barger, K. Whisnant, S. Pakvasa and R. J. N. Phillips, Phys. Rev. D **22**, 2718 (1980).
 - [50] A. Cervera, A. Donini, M. B. Gavela, J. J. Gómez-Cadenas, P. Hernandez, O. Mena and S. Rigolin, Nucl. Phys. B **579**, 17 (2000) [Erratum-ibid. B **593**, 731 (2001)].
 - [51] M. Freund, P. Huber and M. Lindner, Nucl. Phys. B **615**, 331 (2001).
 - [52] C. Ishihara, PoS **NUFACT08**, 044 (2008); For details, see the talk given by Chizue Ishihara at EUROnu annual meeting at CERN, Geneva, 23-27th March, 2009.
 - [53] S. Amerio *et al.* [ICARUS Collaboration], Nucl. Instrum. Meth. A **527**, 329 (2004).
 - [54] Bonnie T. Fleming, private communication.
 - [55] V. Barger, M. Dierckxsens, M. Diwan, P. Huber, C. Lewis, D. Marfatia and B. Viren, Phys. Rev. D **74** (2006) 073004; M. Diwan *et al.*, arXiv:hep-ex/0608023; V. Barger, P. Huber, D. Marfatia and W. Winter, Phys. Rev. D **76**, 031301 (2007); V. Barger, P. Huber, D. Marfatia and W. Winter, Phys. Rev. D **76**, 053005 (2007).
 - [56] M. Bishai, AIP Conf. Proc. **981**, 102 (2008).
 - [57] http://www.fnal.gov/directorate/OPMO/Projects/PP/DirRev/2006/08_15/review.htm

- [58] P. Huber, J. Kopp, M. Lindner, M. Rolinec and W. Winter, *Comput. Phys. Commun.* **177**, 432 (2007); P. Huber, M. Lindner and W. Winter, *Comput. Phys. Commun.* **167**, 195 (2005).
- [59] M. Maltoni, T. Schwetz, M. A. Tortola and J. W. F. Valle, *New J. Phys.* **6**, 122 (2004).
- [60] P. Huber, M. Lindner, T. Schwetz and W. Winter, *JHEP* **0911**, 044 (2009).
- [61] P. Huber, M. Lindner and W. Winter, *Nucl. Phys. B* **645**, 3 (2002).